

# Structural plasticity of pyramidal cell neurons measured after FLASH and conventional dose-rate irradiation

**Dara L. Dickstein**

Uniformed Services University of Health Sciences

**Richard Zhang**

University of California, Irvine School of Medicine

**Ning Ru**

University of California, Irvine School of Medicine

**Marie-Catherine Vozenin**

Hôpitaux Universitaires de Genève

**Bayley C. Perry**

Uniformed Services University of Health Sciences

**Juan Wang**

Uniformed Services University of Health Sciences

**janet baulch**

University of California, Irvine School of Medicine

**Munjal M. Acharya**

University of California, Irvine School of Medicine

**Charles L. Limoli**

`climoli@uci.edu`

University of California, Irvine School of Medicine

---

## Research Article

**Keywords:** FLASH, radiotherapy, cranial irradiation, neuron, structural plasticity

**Posted Date:** July 22nd, 2024

**DOI:** <https://doi.org/10.21203/rs.3.rs-4656938/v1>

**License:**   This work is licensed under a Creative Commons Attribution 4.0 International License.

[Read Full License](#)

**Additional Declarations:** No competing interests reported.

---

# Abstract

Evidence shows that ultra-high dose-rate FLASH-radiotherapy (FLASH-RT) protects against normal tissue complications and functional decrements in the irradiated brain. Past work has shown that radiation-induced cognitive impairment, neuroinflammation and reduced structural complexity of granule cell neurons were not observed to the same extent after FLASH-RT (> MGy/s) compared to conventional dose-rate (CONV, 0.1 Gy/s) delivery. To explore the sensitivity of different neuronal populations to cranial irradiation and dose-rate modulation, hippocampal CA1 and medial prefrontal cortex (PFC) pyramidal neurons were analyzed by electron and confocal microscopy. Neuron ultrastructural analyses by electron microscopy after 10 Gy FLASH- or CONV-RT exposures indicated that irradiation had little impact on dendritic complexity and synapse density in the CA1, but did increase length and head diameter of smaller non-perforated synapses. Similarly, irradiation caused no change in PFC prelimbic/infralimbic axospinous synapse density, but reductions in non-perforated synapse diameters. While irradiation resulted in thinner myelin sheaths compared to controls, none of these metrics were dose-rate sensitive. Analysis of fluorescently labeled CA1 neurons revealed no radiation-induced or dose-rate-dependent changes in overall dendritic complexity or spine density, in contrast to our past analysis of granule cell neurons. Super-resolution confocal microscopy following a clinical dosing paradigm (3×10Gy) showed significant reductions in excitatory vesicular glutamate transporter 1 and inhibitory vesicular GABA transporter puncta density within the CA1 that were largely dose-rate independent. Collectively, these data reveal that, compared to granule cell neurons, CA1 and mPFC neurons are more radioresistant irrespective of radiation dose-rate.

## Introduction

The complexity of the dendritic tree and the interconnections between dendritic spines define a myriad of synaptic capabilities that mediate neurotransmission. In the adult rodent brain, age, disease and cancer treatment-associated changes can compromise the integrity of neuronal structure and adversely impact cognition (Selkoe 2002; Dickstein et al. 2007; Dickstein et al. 2010; Seigers and Fardell 2011; Vogel-Ciernia et al. 2013; Christie et al. 2012; Parihar and Limoli 2013; Dickstein et al. 2013; Baulch et al. 2016). Among these treatment, cranial radiotherapy and systemic chemotherapy represent frontline treatments for forestalling the growth of brain malignancies and disseminated, oligometastatic disease (Evenden 2013; Wefel and Schagen 2012) (Makale et al. 2017). In rodent models, each of these treatments elicits qualitatively similar adverse neurocognitive sequelae invariably associated with elevations in neuroinflammation along with macroscopic changes in dendritic complexity, microscopic changes in synapse morphology and changes in neuronal structural elements including dendritic spines, axonal myelination and synaptic bouton (Acharya et al. 2015a) (Acharya et al. 2015b) (Parihar et al. 2015) (Dickstein et al. 2018) (Allen et al. 2022). The majority of our past work has focused on granule cell neurons in the hippocampal dentate that exhibit exquisite sensitivity to photon, electron and proton irradiation delivered at conventional dose-rates (CONV, 2 Gy/min) (Parihar and Limoli 2013; Parihar et al. 2015; Parihar et al. 2016; Baulch et al. 2016; Montay-Gruel et al. 2019). Studies implementing a wide range of radiation paradigms have shown that doses ranging from 0.3 to 10 Gy elicit marked and

persistent reductions in dendritic arborization, immature dendritic spine density and myelination at protracted 1 to 9 month post-irradiation times (Parihar and Limoli 2013; Parihar et al. 2015; Baulch et al. 2016; Dickstein et al. 2018; Montay-Gruel et al. 2019; Alagband et al. 2023b). Interestingly, when granule cell neurons were analyzed at similar times following exposure to electron FLASH-radiotherapy (FLASH), these same reductions in dendritic complexity and spine density were not found at doses as high as 10 Gy (Montay-Gruel et al. 2019).

While granule cell neurons and the cellular constituents within the neurogenic niches of the mammalian brain have been studied extensively over decades (van Praag et al. 2002) (Tofilon and Fike 2000) (Mizumatsu et al. 2003), differences in the radiosensitivity and structural plasticity of relatively more mature neuronal populations have not. Further, whether mature populations of neurons exhibit sensitivity to changes in dose-rate that characterize CONV and FLASH irradiation modalities remain equally unexplored. Post-mitotic neurons comprising the majority of the brain have been studied in aging and neurodegenerative conditions using combinations of fluorescently-labeled mouse models (Parihar and Limoli 2013), dye loading (Price et al. 2014) and electron microscopic (EM) techniques (Bloss et al. 2013). These approaches have been used by our group to characterize radiation-induced changes in the hippocampal dentate (Parihar and Limoli 2013; Price et al. 2014), but not for principal cells in other regions of the brain or after exposure to CONV and FLASH electron radiations. Thus, the focus of the current study was twofold, **1)** to address whether relatively mature and arbored subsets of neurons in the pyramidal layer of the CA1 and prelimbic/infralimbic region of the medial prefrontal cortex (PFC) exhibited similar sensitivities to radiation exposure and **2)** whether they were responsive to dose-rate modulation as observed for granule cell neurons (Montay-Gruel et al. 2019). Ultrastructural analyses of both neuronal populations by EM showed these neurons to be largely resistant to radiation-induced change, findings that were corroborated by analysis of fluorescently labeled neurons in the CA1 by confocal microscopy. Furthermore, while analyses of excitatory vesicular glutamate transporter 1 and inhibitory vesicular GABA transporter (*i.e.* glutamatergic/GABAergic VGLUT/VGAT) puncta in the CA1 revealed dose-dependent reductions in synapse density, they were not found to depend on dose-rate. Here we report on the marked radioresistance of pyramidal neurons to structural alterations following clinically relevant radiation doses delivered at either CONV or FLASH dose-rates.

## Materials and Methods

### Animals and irradiations

Animal experiments were approved by the Swiss (Vaud state approval: VD2920, 3241 and 3603) and University of California, Irvine (Institutional Animal Care and Use Committee: AUP 23–080) ethics committees for animal experimentation and follow ARRIVE guidelines and address the 10 essential criteria described therein.

Female C57Bl6/J mice were purchased from Charles River Laboratories at 8 weeks of age. Tumor-free female transgenic mice (Tg(Thy1-eGFP) MJrsJ, stock no. 007788; The Jackson Laboratory) were bred at

the University of California, Irvine animal facility. Mice received whole-brain irradiations (WBI) using the Oriatron eRT6 (PMB-Alcen) at 10 Gy, under isoflurane anesthesia where the mouse head was positioned behind and in contact with the aperture of the 1.7-cm-diameter graphite applicator to irradiate the brain at either CONV dose-rate (0.09 Gy/second) or ultra-high dose-rate FLASH delivered in a single 1.8  $\mu$ s pulse ( $5.6 \times 10^6$  Gy/second) thus irradiating the whole encephalon region, while limiting the dose to the eyes, the mouth, and the rest of the body (Montay-Gruel et al. 2017). The brains of mice were prepared for EM and confocal microscopy 6 months after irradiation.

## Neuronal reconstruction

For 3-dimensions neuronal reconstructions, intracellular injections of individual CA1 hippocampal neurons were performed as previously described (Krishnan et al. 2021; Dickstein et al. 2018). Briefly, sections were incubated in 4',6-diamidino-2-phenylindole (DAPI; Vector Labs) to reveal the cytoarchitectural features of the pyramidal layer of the CA1. The sections were mounted on nitrocellulose paper, immersed in ice-cold 0.1 M PBS and pyramidal neurons were subjected to an intracellular iontophoretic injection of 5% Lucifer Yellow (Invitrogen) under a direct current of 3–8 nA until dye had completely filled distal processes (Krishnan et al. 2021; Price et al. 2014; Steele et al. 2014). Five to 10 neurons were injected per slice and placed far enough apart to avoid overlapping of their dendritic trees. Brain sections were then mounted on gelatin-coated glass slides and cover slipped in Fluoromount G slide-mounting media (Southern Biotech).

Intact filled neurons were manually traced and reconstructed in with a 63 $\times$ /1.4 N.A., Plan-Apochromat oil immersion objective on a Zeiss Axio Imager Vario microscope equipped with a motorized stage, video camera system, and Neurolucida morphometry software (MBF Bioscience). To be included in the analysis, a loaded neuron had to satisfy the following criteria: **1)** reside within the pyramidal layer of the CA1 as defined by cytoarchitectural characteristics; **2)** demonstrate complete filling of dendritic tree, as evidenced by well-defined endings; and **3)** demonstrate intact tertiary branches, with the exception of branches that extended beyond 50  $\mu$ m in radial distance from the cell soma (Krishnan et al. 2021; Price et al. 2014; Steele et al. 2014). Using NeuroExplorer software (MBF Bioscience) total dendritic length, number of intersections, and the amount of dendritic material per radial distance from the soma, in 30- $\mu$ m increments (Sholl 1953), were analyzed in order to assess morphological cellular diversity and potential differences between the animal groups. A total of 50 cells were reconstructed for controls (~ 8 cells per animal) and a total of 49 cells were reconstructed for the irradiated mice (~ 8 cells per animal).

### Ultrastructural analysis of synapses and myelinated axons with electron microscopy

Coronal sections encompassing the CA1 region of the hippocampus and the medial PFC were prepared for EM as reported previously (Krishnan et al. 2021; Price et al. 2014; Steele et al. 2014; Alaghband et al. 2023b; Dickstein et al. 2018). Brain slices (250  $\mu$ m-thick) were cryoprotected in graded phosphate buffer/glycerol washes at 4°C, manually microdissected into 1 mm blocks, rapidly freeze-plunged into liquid propane cooled by liquid nitrogen (– 190°C) in a universal cryofixation system KF80 (Reichert-Jung, Leica Microsystems, Wetzlar, Germany) and subsequently immersed in 1.5% uranyl acetate dissolved in

anhydrous methanol at  $-90^{\circ}\text{C}$  for 24 hr in a cryosubstitution unit (Leica). Block temperatures were raised from  $-90$  to  $-45^{\circ}\text{C}$  in steps of  $4^{\circ}\text{C}$  per hour. Blocks were washed with anhydrous methanol, and infiltrated with Lowicryl resin (Electron Microscopy Sciences) at  $-45^{\circ}\text{C}$ , polymerized by exposure to ultraviolet light (360 nm) for 48 hr at  $-45^{\circ}\text{C}$  followed by 24 hr at  $0^{\circ}\text{C}$ . Block faces were trimmed and ultrathin sections (90 nm) were cut with a diamond knife (Diatome) on an ultramicrotome (Reichert-Jung). Tissue grids were imaged on a JEOL JEM-1011 TEM (JEOL USA Inc, Peabody, MA) with an AMT XR50S-A camera (Advanced Microscopy. Techniques, Woburn, MA).

For synapse quantification, serial section micrographs were imaged at  $15,000\times$ . An unbiased stereological approach using the physical disector was performed to measure synapse density, as described in our previous work (Lazarczyk et al. 2023; Krishnan et al. 2021; Alaghband et al. 2023b; Dickstein et al. 2018). Nine sets of serial images across the same set of five consecutive ultrathin sections were taken for each animal and imported into Adobe Photoshop (version CC 2018 19.1.2, Adobe Systems, San Jose, CA). All axospinous synapses were identified within the first two and the last two images of each five-section serial set, and counted if they were contained in the reference image but not in the corresponding look-up image. To increase sampling efficiency, the reference image and look-up image were then reversed, thus each animal included in the current study contributed synapse density data from a total of 18 disector pairs. Axospinous synapse density was calculated as the total number of unique counted synapses from both images divided by the total volume of the disector (area  $\times$  height of disector). The criteria for inclusion as an axospinous synapse included the presence of a presynaptic terminal and a distinct PSD separated by a clear synaptic cleft. The same volume was sampled for each group. In addition to total synapse density, we also measured the densities of nonperforated and perforated synapses. Perforated synapses were defined by the presence of a discontinuity in the PSD. A single person, blinded to each of the treatment groups, performed all analyses.

Quantification of myelination was performed as previously described (Dickstein et al. 2018; Krishnan et al. 2021; Alaghband et al. 2023b). Briefly, to characterize the degree of myelination, the numbers of myelinated and unmyelinated axons were counted in 12 randomly selected, nonoverlapping fields of the hippocampal sulcus from each animal at  $10,000\times$ . Both the number of myelinated axons per square millimeter and the percent of total myelinated axons were calculated. An additional six randomly selected, nonoverlapping images were taken per animal at  $15,000\times$  to evaluate myelin sheath thickness through g-ratio analysis. Four measurements were recorded for each myelinated axon: the longest axon diameter, the shortest axon diameter, the longest myelin width, and the shortest myelin width. To calculate the g-ratio, the average diameter for each axon was divided by the average axon diameter plus twice the average myelin width (Dupree et al. 2015; Murcia-Belmonte et al. 2016). Myelin regions that exhibited fixation artifacts or noncompaction were excluded from the analysis. A single person, blinded to the treatment groups, performed all analyses.

## **Immunohistochemistry, Confocal Microscopy, and Quantification**

Hemizygous *Thy1-EGFP* mice expressing eGFP provided a fluorescent signal facilitating neuronal micromorphometric analysis as described previously (Parihar and Limoli 2013; Parihar et al. 2015). Briefly, 100 µm-thick hippocampal sections were cut for dendritic confocal imaging and analysis using a cryostat (Leica Microsystems). Three sections per animal were used to generate Z-stacks from four animals using a Nikon C2 confocal microscope. Images comprising each Z-stack ( $1,024 \times 1,024$  pixels) were acquired (100×) over the entire dendrite tree at 0.25-µm increments. Detailed dendritic tracing and spine classification was performed using the Imaris 10.1 software suite (Bitplane, Inc./Oxford Instruments). For spines to be included in our analyses, they required a minimal length of 0.3 µm and a maximal length of 1.8 µm. Parameters of neuronal structure that were identified and quantified through image reconstruction and deconvolution using the Imaris software suite included the cell body, dendritic and axonal length, branching and branch points, dendritic complexity, spines, and boutons.

Animals were prepared for immunohistochemistry as described previously (Allen et al. 2022; Alaghband et al. 2023a). Briefly, brains were sectioned coronally (30–35 µm thick) using a cryostat (Leica Microsystems) for super resolution microscopy and two 30 µm sections per animal containing the dorsal hippocampus were washed with PBS, before being permeabilized in a solution of 0.3% TX-100. Sections were then blocked in a solution of 10% NGS in PBS with 0.3% TX-100 and 4% BSA for 1 hour and incubated overnight with VGLUT and VGAT primary antibodies (1:500, Synaptic Systems, Cat No. 135304, Cat No. 131003), in a solution of 0.3% TX-100, 10% NGS, and 1x PBS. Sections were then washed and incubated with secondary antibodies (1:1000 Invitrogen Anti-Guinea Pig AlexaFluor 488 A11073, 1:1000 Invitrogen Goat Anti-Rabbit AlexaFluor 555 A21428), before counterstaining with DAPI, and mounting. Sections were imaged at 63× on an Elyra 7 Super resolution microscope (Zeiss), focused on the apical CA1 region of the hippocampus. Images were captured at a resolution of  $1280 \times 1280$  comprising of a Z-stack consisting of images taken at 273 nm intervals. Images were then processed using the Zeiss Zen Black Software's SIM<sup>2</sup> feature, to create super-resolution images of VGLUT and VGAT Puncta. Puncta were then quantified using Imaris 10.1 image analysis software via the Spots function. Spots larger than 180 nm were identified as puncta and counted. The number of puncta observed were averaged per animal, for a total of 8 animals per treatment.

## Statistics

For neuronal structure analyses, following confirmation of normal Gaussian distribution, one-way ANOVAs were used to assess significance between control and irradiated groups. A Tukey's post hoc test was used to compare CONV-RT and FLASH-RT groups against the control group when overall group effects were found to be statistically significant. Two-way repeated measures were performed for Sholl analyses. For synapse density (total, perforated and non-perforated), following confirmation of normal Gaussian distribution, we performed one-way ANOVAs followed by Tukey's multiple comparison when significance was achieved. The  $\alpha$  level was set at 0.05 with values of  $p < 0.05$  considered statistically significant. All data are reported as mean  $\pm$  SEM. Statistical significance was calculated using GraphPad Prism 8 (San Diego, CA).

For the myelin analysis, to account for the nested data produced by g-ratio quantification, differences between treatment groups were evaluated using a linear mixed-effect model (LMM) regression analysis approach. LMMs were fit in R 4.1.2 using the lme4 (Bates et al. 2015) and lmerTest (Kuznetsova et al. 2017) packages, where outcome measures were analyzed against treatment fixed effects and a random effect for animal ID, representing the nested variation from multiple synapse or axon measurements per animal. Significant interaction effects were decomposed by comparison of estimated marginal means with the demmeans package in R (Length 2022). Results were expressed as mean  $\pm$  SEM and all analyses considered a value of  $p < 0.05$  to be statistically significant.

## Results

### Radiation treatment does not affect neuronal complexity

We assessed whether CA1 neurons from FLASH and CONV irradiated mice would display differences in dendritic length and complexity compared to neurons from control mice. A total of 14 animals and a minimum of 5 neurons per animal met the inclusion criteria for use in neuronal reconstructions (Table 1). Representative examples of CA1 dendritic arbor reconstructions of FLASH, CONV and control neurons are depicted in Fig. 1a. We found no significant difference in apical or basal dendritic length between all three treatment groups (apical:  $F_{(2,11)} = 0.22$ ;  $p = 0.81$  and basal:  $F_{(2,11)} = 0.53$ ,  $p = 0.60$ , one-way ANOVA; Fig. 1b, e). We then performed a Sholl analysis to identify any further changes in morphological complexity that may occur in response to different radiation treatments. When comparing the numbers of intersections and the amount of dendritic length at specific distances from the soma on both apical and basal dendrites, we found no significant main effect of treatment (Fig. 1c, d and g, h).



Table 1

Summary of the numbers and quantitative morphological data of neurons, synapses and myelinated axons analyzed for each treatment group derived from EM.

<b>CA1 neuron morphology</b>			
Parameter	Control	CONV	FLASH
Number of Animals	4	5	5
Number of neurons	24	30	31
<b>CA1 Synapses</b>			
Parameter	Control	CONV	FLASH
	Mean $\pm$ SEM	Mean $\pm$ SEM	Mean $\pm$ SEM
Number of Animals			
Synapse density (synapses/mm <sup>3</sup> )			
Total	2.375 $\pm$ 0.202	2.839 $\pm$ 0.101	2.831 $\pm$ 0.153
Perforated synapse density	0.413 $\pm$ 0.039	0.405 $\pm$ 0.056	0.410 $\pm$ 0.018
Non-perforated synapse density	2.32 $\pm$ 0.169	2.434 $\pm$ 0.086	2.420 $\pm$ 0.146
PSD length	0.230 $\pm$ 0.003	0.225 $\pm$ 0.002	0.232 $\pm$ 0.003
PSD Area	0.037 $\pm$ 0.04	0.031 $\pm$ 0.001	0.033 $\pm$ 0.001
Spine head diameter	0.376 $\pm$ 0.06	0.374 $\pm$ 0.008	0.377 $\pm$ 0.005
<b>PFC Synapses</b>			
Parameter	Control	CONV	FLASH
	Mean $\pm$ SEM	Mean $\pm$ SEM	Mean $\pm$ SEM
Number of animals	5	5	5
Synapse density (synapses/mm <sup>3</sup> )			
Total	1.117 $\pm$ 0.086	1.067 $\pm$ 0.050	1.017 $\pm$ 0.084
Perforated synapse density	0.220 $\pm$ 0.021	0.171 $\pm$ 0.006	0.159 $\pm$ 0.026
Non-perforated synapse density	0.896 $\pm$ 0.077	0.896 $\pm$ 0.050	0.856 $\pm$ 0.063
PSD length (mm)	0.312 $\pm$ 0.012	0.279 $\pm$ 0.003	0.283 $\pm$ 0.008
PSD Area (mm)	0.025 $\pm$ 0.001	0.022 $\pm$ 0.001	0.023 $\pm$ 0.001
Spine head diameter (mm <sup>2</sup> )	0.523 $\pm$ 0.017	0.443 $\pm$ 0.005	0.459 $\pm$ 0.008

CA1 neuron morphology			
Myelin			
Animals	5	5	5
Number myelinated axons counted	2392	1939	1906
Number of axons for g-ratio	530	607	503

Table 2  
Summary of the numbers and quantitative morphological data of neurons and synapses for each treatment group derived from EGFP-labeled brain sections.

	Control	CONV	FLASH
	(Mean $\pm$ SEM)	(Mean $\pm$ SEM)	(Mean $\pm$ SEM)
Spine Head Diameter	0.51 $\pm$ 0.021	0.6 $\pm$ 0.02	0.54 $\pm$ 0.02
Dendritic Branches	4.43 $\pm$ 0.39	3.46 $\pm$ 0.32	3.93 $\pm$ 0.43
Dendritic Area	1135.17 $\pm$ 139.60	1020.27 $\pm$ 115.96	1075.17 $\pm$ 108.32
Spine Volume	40.83 $\pm$ 7.20	56.84 $\pm$ 17.44	62.62 $\pm$ 18.83
Filament Volume	202.55 $\pm$ 27.00	250.20 $\pm$ 33.48	245.20 $\pm$ 28.65
Filament Length	453.71 $\pm$ 47.63	365.35 $\pm$ 35.92	409.50 $\pm$ 40.08
Spine Count	242.17 $\pm$ 32.32	205.85 $\pm$ 26.98	216.20 $\pm$ 23.93

### Radiation affects synapse morphology but not density in the CA1 region of the hippocampus and mPFC

To study the axospinous synapse density in the *stratum radiatum* (SR) region of the hippocampus, total synapse density as well as the density of perforated and non-perforated synapses were examined. Approximately 11,202 synapses were counted from all groups (747 spines per animal on average) across 9 serial EM sections using the dissector method (Table 1). Analysis of total synapse density revealed no significant differences between control ( $2.735 \pm 0.202$  synapses/ $\mu\text{m}^3$ ), CONV ( $2.839 \pm 0.101$  synapses/ $\mu\text{m}^3$ ) and FLASH mice ( $2.831 \pm 0.153$  synapses/ $\mu\text{m}^3$ ) (Fig. 2a). The density of different types of synapses, perforated versus non-perforated, was assessed further. Neither CONV nor FLASH treatments changed the density of perforated synapses compared to control mice ( $0.413 \pm 0.039$ ), CONV ( $0.405 \pm 0.056$ ) and FLASH mice ( $0.410 \pm 0.018$ ) perforated synapses/ $\mu\text{m}^3$  or non-perforated synapses compared to control mice  $2.321 \pm 0.169$ , CONV  $2.434 \pm 0.086$ , FLASH  $2.420 \pm 0.146$  non-perforated synapses/ $\mu\text{m}^3$ ) (Fig. 2b, c). We next examined the length and area of the PSD as well as the head diameter of individual spines. In regards to PSD length, there was difference between the groups (Fig. 2d). Measurement of spine head diameter also revealed no significant difference between control and CONV or FLASH mice (Fig. 2g). Our previous studies have classified mouse spines with head diameters  $< 0.4 \mu\text{m}$  as thin spines

and  $> 0.4 \mu\text{m}$  as mushroom spines (Dickstein et al. 2018; Krishnan et al. 2021; Lazarczyk et al. 2016; Price et al. 2014; Steele et al. 2014). We applied this parameter to the PSD length and head diameter to non-perforated and perforated synapses. We found no difference in PSD length between groups in perforated synapses but did observe significant differences in non-perforated synapses. In particular, in synapses  $< 0.4 \mu\text{m}$  CONV treated animals had smaller PSD than sham controls ( $F_{(2, 3571)} = 3.570$ ,  $p = 0.028$ ; Fig. 2f), while synapses  $> 0.4 \mu\text{m}$  both CONV and FLASH treated animals had larger PSDs compared to SHAM controls ( $F_{(2, 1649)} = 27.30$ ,  $p < 0.0001$ ; Fig. 2f). When we examined head diameter, CONV treated mice had significantly larger head diameters compared to controls in perforated synapses ( $F_{(2, 471)} = 4.246$ ,  $p = 0.015$ ; Fig. 2h). There was no difference in head diameter in non-perforated synapses (Fig. 2i).

As was done for the hippocampus, we also examined the axospinous synapse density in the prelimbic/infralimbic region of the mPFC. Approximately 6502 unique synapses were studied from all groups ( $\sim 507$  synapses per animal  $n = 5$  animals/group; see Table 1 for synapse measurements). Analysis of total synapse density revealed no significant differences between control mice, CONV mice and FLASH mice ( $F_{(2, 12)} = 0.663$ ,  $p = 0.533$ , one-way ANOVA; Fig. 3a). The density of different types of synapses, perforated versus non-perforated, was assessed further. While CONV mice seemed to have a similar perforated synapse density as controls, FLASH-treated mice had fewer perforated synapses, this difference did not reach significance ( $F_{(2, 12)} = 1.358$ ,  $p = 0.294$ , one-way ANOVA; Fig. 3b). There was no significant difference in non-perforated synapse density among groups ( $F_{(2, 12)} = 0.2372$ ,  $p = 0.7924$ , one-way ANOVA; Fig. 3c). We next examined PSD length as well as the head diameter (HD) of the spine. We found no difference in overall length of the PSD in the irradiated mice compared to control mice ( $F_{(2, 12)} = 1.259$ ,  $p = 0.3188$ , one-way ANOVA; Fig. 3d). Measurement of spine head diameter revealed a significant difference between groups ( $F_{(2, 12)} = 5.480$ ,  $p = 0.020$ , one-way ANOVA; control vs CONV:  $p = 0.017$ , Control vs FLASH:  $p = 0.129$ , Bonferroni's multiple comparison tests, Fig. 3g). When separating synapses by size as performed above, we found that there was no difference in perforated PSD length ( $F_{(2, 253)} = 0.8765$ ,  $p = 0.4175$ , one-way ANOVA, Fig. 3e) but a significant difference in HD ( $F_{(2, 253)} = 3.353$ ,  $p = 0.036$ ; Fig. 3h). When we looked at the PSD length of non-perforated synapses we found that there was no difference in larger spines  $> 0.4 \mu\text{m}$  ( $F_{(2, 1321)} = 0.840$ ,  $p = 0.432$ ; Fig. 3f) but did see significant differences in smaller spines with FLASH treated mice having smaller PSDs than control and CONV treated mice ( $F_{(2, 1158)} = 5.190$ ,  $p = 0.006$ , Control vs FLASH:  $p = 0.019$ , CONV vs FLASH:  $p = 0.01$ , Bonferroni's multiple comparison tests; Fig. 3f). We also saw significant differences in HD. In synapses  $< 0.4 \mu\text{m}$  both CONV and FLASH treated mice had smaller HD than controls ( $F_{(2, 1193)} = 94.28$ ,  $p < 0.0001$ , control vs CONV:  $p < 0.0001$ , Control vs FLASH:  $p < 0.0001$ , Bonferroni's multiple comparison tests; Fig. 3h). For HD  $> 0.4 \mu\text{m}$ , irradiate mice had smaller HD ( $F_{(2, 1344)} = 4.964$ ,  $p = 0.007$ , control vs CONV:  $p = 0.006$ , Control vs FLASH:  $p = 0.797$ , Bonferroni's multiple comparison tests; Fig. 3i).

**FLASH and CONV mice have thinner myelin sheaths than controls.**

We analyzed the morphology of axons in all three groups of mice (Table 1). Representative images of myelinated axons are depicted in Fig. 4a **and b**. We found that CONV treatment restored the percent of myelinated axons to levels similar to controls while FLASH treated animals had fewer myelinated axons, however these changes did not reach significance ( $F_{(2, 12)} = 3.518$ ,  $p = 0.079$ , one-way ANOVA; Table 1, Fig. 4c). We then measured the mean g-ratio (the ratio between the diameter of an axon and the diameter of the fiber including myelin) for all axons. We did observe that the myelin sheath of irradiated mice was thinner than control as seen by a larger g-ratio value. In particular, the g-ratio of FLASH irradiated fibers was significantly increased when compared with controls indicating a thinner myelin sheath ( $F_{(2, 1637)} = 6.477$ ,  $p = 0.002$ , one-way ANOVA; control vs CONV:  $p = 0.051$ , Control vs FLASH:  $p = 0.001$ , Tukey's multiple comparison tests, Fig. 4d). When we analyzed g-ratio within classes of fibers binned for their axonal diameter, decreased myelin thickness was present for all diameter sizes for both CONV and FLASH irradiated animals compared to controls (diameter < 0.4 mm:  $F_{(2, 502)} = 55.61$ ,  $p = 0.0001$ , one-way ANOVA, control vs CONV:  $p < 0.0001$ , Control vs FLASH:  $p < 0.0001$ , Tukey's multiple comparison tests; diameter 0.4–0.6 mm:  $F_{(2, 706)} = 70.57$ ,  $p < 0.0001$ , one-way ANOVA, control vs CONV:  $p < 0.0001$ , Control vs FLASH:  $p < 0.0001$ , Tukey's multiple comparison tests; diameter 0.6–0.8 mm:  $F_{(2, 1039)} = 17.12$ ,  $p < 0.0001$ , one-way ANOVA, control vs CONV:  $p = 0.026$ , Control vs FLASH:  $p < 0.0001$ , CONV vs FLASH:  $p = 0.0002$ , Tukey's multiple comparison tests; diameter > 0.8 mm:  $F_{(2, 105)} = 4.998$ ,  $p = 0.008$ , one-way ANOVA, control vs CONV:  $p = 0.02$ , Control vs FLASH:  $p < 0.02$ , Tukey's multiple comparison tests; Fig. 4e).

### **Dendritic complexity and spine density is not affected by radiation dose or dose-rate.**

Using Thy1-eGFP-expressing mice exposed to CONV and FLASH RT, we analyze CA1 pyramidal neuronal spine density, number of dendritic branches and dendritic (filament) volume within the apical dendrites in the SR (Fig. 5). This analysis was facilitated by Imaris (v10) filament reconstruction module as described previously (Parihar/BSF). We did not find significant differences in spine density per 100  $\mu\text{m}$  of the dendritic section following either CONV or FLASH- dose-rate irradiations (Fig. 5A). Similarly, we did not find statistical significance between unirradiated controls, CONV- or FLASH-RT for dendritic parameters including dendritic branch numbers and dendritic volume.

### **Excitatory/inhibitory synapse density is not altered by radiation dose or dose-rate.**

To determine the impact to cranial irradiation and dose-rates on inhibitory and excitatory vesicular trafficking markers, immunofluorescence staining, super resolution microscopy, and 3D algorithm-based volumetric quantification of immunoreactive puncta for excitatory vesicular glutamate transporter 1 (VGLUT) and inhibitory vesicular GABA transporter (VGAT) was conducted within the CA1 *stratum radiatum* of Thy1-eGFP mice exposed to cranial irradiation (Fig. 6). We found a significant decline in number of VGAT and VGLUT immunoreactive puncta following 10 Gy of either CONV ( $p < 0.0001$ ) or FLASH ( $p < 0.0001$ ) irradiation compared to unirradiated controls in male animals (Fig. 6A-B). Additionally, we did not find significant differences between CONV and FLASH dose-rates for the number of VGAT and VGLUT puncta (Fig. 6B).

## Discussion

In the present study, we used ultrastructural analyses of neuronal populations by EM and analysis of fluorescently labeled neurons in the CA1 by confocal microscopy to investigate the impact of radiation exposure and dose rate modulation on mature and arbored subsets of neurons located in the pyramidal layer of the CA1 and prelimbic/infralimbic region of the medial prefrontal cortex (PFC). We found that these pyramidal neurons are radiation resistant and dose rate insensitive, while analyses of excitatory vesicular glutamate transporter 1 and inhibitory vesicular GABA transporter (*i.e.* glutamatergic/GABAergic VGLUT/VGAT) puncta in the CA1 revealed dose-dependent reductions in synapse density, they were not found to depend on dose-rate.

The mechanisms underlying radiation-induced cognitive dysfunction are complex and multifactorial, involving multiple cellular subtypes that directly and indirectly regulate neurotransmission. As direct mediators of this process, neurons are central candidates, and the temporal coincidence between radiation-induced cognitive decrements and changes in neuronal structure provides for one plausible explanation. A logical extension of this tenet would presume that different neurons across various regions of the brain would exhibit different sensitivities to such change, and data here supports that idea, where pyramidal cell neurons in the CA1 and PFC were more resistant to radiation-induced reductions in dendritic morphology compared to granule cell neurons in the hippocampal dentate detailed in a prior study (Montay-Gruel et al. 2019). The foregoing was corroborated using two independent techniques for quantifying morphologic parameters, where dendritic complexity and spine density of dye loaded and intrinsically fluorescent pyramidal cell neurons were also relatively unaffected by changes in dose-rate. While changes in non-perforated synapses were found in the irradiated cohorts analyzed by EM, ascribing how such alterations might impact the wide range of behavioral tasks analyzed in our past CONV and FLASH radiation studies remains uncertain. Radiation exposure was found to reduce the density of VGLUT/VGAT synapse density, and while trends pointed to a preservation of this loss after FLASH-RT, significance was not found across the cohorts analyzed.

While this investigation sought to uncover whether distinct neuronal populations exhibited differences in radiation-induced structural plasticity, it also sought to determine whether such changes were dose-rate dependent. Here, the radioresistance of pyramidal cell structural plasticity precluded demonstration of FLASH sparing of the morphologic determinates evaluated in the CA1 and mPFC. Past work implementing time-lapsed 2-photon microendoscopy in the CA1 of live mice has shown the temporal dynamics of dendritic spine turnover to differ across brain regions (Berry and Nedivi 2017), suggesting that the transience of hippocampal-dependent memory is linked to the turnover of hippocampal synapses ((Attardo et al. 2015), reviewed in (Berry and Nedivi 2017)). Several studies focused on aging and neurodegeneration have linked changes in dendritic spine morphology to functional impairments and cognition (Bloss et al. 2011; Bloss et al. 2010; Bloss et al. 2013);Price, 2014 #3180;Steele, 2014 #2620;Boros, 2017 #4065]. Irradiation is likely to alter basal turnover rates of many critical synaptic elements across the entire brain and given the protracted nature of such changes it is hard to dismiss

the relationship between neuronal morphology and cognition. Clearly many cellular mechanisms converge to impact cognition, and the benefits of FLASH-RT cannot be solely linked to the integrity of the dendritic tree, synapse density or morphology across different neuronal populations. While the unique memory sparing capabilities of FLASH radiotherapy have provided a potentially new avenue for resolving quality of life concerns in brain tumor survivors, such benefits likely extend beyond neuronal structure and across multiple cell types in the brain.

## **Declarations**

### **Author contributions**

All authors commented on previous versions of the manuscript and read and approved the final manuscript.

### **Funding**

This work was supported by the National Institutes for Health (NIH) awards P01 CA244091 (CLL, MCV), R01 CA254892 (CLL, MCV), NINDS R01NS089575 (CLL, DLD) and R01 CA251110 (MMA).

### **Data availability**

The datasets generated during and/or analysed during the current study are available from the corresponding author on reasonable request.

## **Disclaimer**

The opinions expressed herein are those of the authors and are not necessarily representative of those of the government of the United States, the Uniformed Services University of the Health Sciences, the Department of Defense (DoD), or the United States Army, Navy or Air Force or the Henry M. Jackson Foundation for the Advancement of Military Medicine Inc.

### **Ethical approval**

All experiments were approved by the Swiss (Vaud state approval: VD2920, VD3241, VD3603 and) and University of California, Irvine (Institutional Animal Care and Use Committee: AUP 23-080) ethics committees for animal experimentation and follow ARRIVE guidelines and address the 10 essential criteria described therein.

### **Competing interests**

The authors have no relevant financial or non- financial interests to disclose.

### **Open Access**

This article is licensed under a Creative Commons Attribution 4.0 International License, which permits use, sharing, adaptation, distribution and reproduction in any medium or format, as long as you give appropriate credit to the original author(s) and the source, provide a link to the Creative Commons license, and indicate if changes were made. The images or other third-party material in this article are included in the article's Creative Commons license, unless indicated otherwise in a credit line to the material. If material is not included in the article's Creative Commons license and your intended use is not permitted by statutory regulation or exceeds the permitted use, you will need to obtain permission directly from the copyright holder. To view a copy of this license, visit <http://creativecommons.org/licenses/by/4.0/>.

## References

1. Acharya MM, Martirosian V, Chmielewski NN, Hanna N, Tran KK, Liao AC, Christie LA, Parihar VK, Limoli CL (2015a) Stem cell transplantation reverses chemotherapy-induced cognitive dysfunction. *Cancer Res* 75(4):676–686. 10.1158/0008-5472.CAN-14-2237
2. Acharya MM, Rosi S, Jopson T, Limoli CL (2015b) Human neural stem cell transplantation provides long-term restoration of neuronal plasticity in the irradiated hippocampus. *Cell Transpl* 24(4):691–702. 10.3727/096368914X684600
3. Alaghband Y, Allen BD, Kramar EA, Zhang R, Drayson OGG, Ru N, Petit B, Almeida A, Doan N-L, Wood MA, Baulch JE, Ballesteros-Zebadua P, Vozenin M-C, Limoli CL (2023a) Uncovering the protective neurologic mechanisms of hypofractionated FLASH radiotherapy. *Cancer Res Comm* 3(4):1–13. 10.1158/2767–9764.CRC-23-0117
4. Alaghband Y, Klein PM, Kramar EA, Cranston MN, Perry BC, Shelerud LM, Kane AE, Doan NL, Ru N, Acharya MM, Wood MA, Sinclair DA, Dickstein DL, Soltesz I, Limoli CL, Baulch JE (2023b) Galactic cosmic radiation exposure causes multifaceted neurocognitive impairments. *Cell Mol Life Sci* 80(1):29. 10.1007/s00018-022-04666-8
5. Allen BD, Alaghband Y, Kramar EA, Ru N, Petit B, Grilj V, Petronek MS, Pulliam CF, Kim RY, Doan NL, Baulch JE, Wood MA, Bailat C, Spitz DR, Vozenin MC, Limoli CL (2022) Elucidating the neurological mechanism of the FLASH effect in juvenile mice exposed to hypofractionated radiotherapy. *Neurooncology*. 10.1093/neuonc/noac248
6. Attardo A, Fitzgerald JE, Schnitzer MJ (2015) Impermanence of dendritic spines in live adult CA1 hippocampus. *Nature* 523(7562):592–596. 10.1038/nature14467
7. Bates D, Mächler M, BM B, Walker S (2015) Fitting linear mixed-effects models using lme4. *J Stat Softw* 67:1–48
8. Baulch JE, Acharya MM, Allen BD, Ru N, Chmielewski NN, Martirosian V, Giedzinski E, Syage A, Park AL, Benke SN, Parihar VK, Limoli CL (2016) Cranial grafting of stem cell-derived microvesicles improves cognition and reduces neuropathology in the irradiated brain. *Proc Natl Acad Sci U S A* 113(17):4836–4841. 10.1073/pnas.1521668113

9. Berry KP, Nedivi E (2017) Spine Dynamics: Are They All the Same? *Neuron* 96(1):43–55. 10.1016/j.neuron.2017.08.008
10. Bloss E, Morrison J, Hof P, Dickstein D (2011) Influence of aging and neurodegeneration on dendritic spine morphology. *Translational Neuroscience* 2(1):49–60
11. Bloss EB, Janssen WG, McEwen BS, Morrison JH (2010) Interactive effects of stress and aging on structural plasticity in the prefrontal cortex. *J Neurosci* 30(19):6726–6731. 10.1523/JNEUROSCI.0759-10.2010
12. Bloss EB, Puri R, Yuk F, Punsoni M, Hara Y, Janssen WG, McEwen BS, Morrison JH (2013) Morphological and molecular changes in aging rat prelimbic prefrontal cortical synapses. *Neurobiol Aging* 34(1):200–210. 10.1016/j.neurobiolaging.2012.05.014
13. Christie LA, Acharya MM, Parihar VK, Nguyen A, Martirosian V, Limoli CL (2012) Impaired cognitive function and hippocampal neurogenesis following cancer chemotherapy. *Clin cancer research: official J Am Association Cancer Res* 18(7):1954–1965. 10.1158/1078-0432.CCR-11-2000
14. Dickstein DL, Brautigam H, Stockton SD Jr., Schmeidler J, Hof PR (2010) Changes in dendritic complexity and spine morphology in transgenic mice expressing human wild-type tau. *Brain Struct Funct* 214(2–3):161–179. 10.1007/s00429-010-0245-1
15. Dickstein DL, Kabaso D, Rocher AB, Luebke JI, Wearne SL, Hof PR (2007) Changes in the structural complexity of the aged brain. *Aging Cell* 6(3):275–284. 10.1111/j.1474-9726.2007.00289.x
16. Dickstein DL, Talty R, Bresnahan E, Varghese M, Perry B, Janssen WGM, Sowa A, Giedzinski E, Apodaca L, Baulch J, Acharya M, Parihar V, Limoli CL (2018) Alterations in synaptic density and myelination in response to exposure to high-energy charged particles. *J Comp Neurol* 526(17):2845–2855. 10.1002/cne.24530
17. Dickstein DL, Weaver CM, Luebke JI, Hof PR (2013) Dendritic spine changes associated with normal aging. *Neuroscience* 251:21–32. 10.1016/j.neuroscience.2012.09.077
18. Dupree JL, Polak PE, Hensley K, Pelligrino D, Feinstein DL (2015) Lanthionine ketimine ester provides benefit in a mouse model of multiple sclerosis. *J Neurochem* 134(2):302–314. 10.1111/jnc.13114
19. Evenden J (2013) Cognitive impairments and cancer chemotherapy: translational research at a crossroads. *Life Sci* 93(17):589–595. 10.1016/j.lfs.2013.03.020
20. Krishnan B, Natarajan C, Bourne KZ, Alikhani L, Wang J, Sowa A, Groen K, Perry B, Dickstein DL, Baulch JE, Limoli CL, Britten RA (2021) Chronic Low Dose Neutron Exposure Results in Altered Neurotransmission Properties of the Hippocampus-Prefrontal Cortex Axis in Both Mice and Rats. *Int J Mol Sci* 22(7). 10.3390/ijms22073668
21. Kuznetsova A, Brockhoff PB, Christensen RHB (2017) lmerTest Package: Tests in Linear Mixed Effects Models. *J Stat Softw* 82(13):1–26
22. Lazarczyk MJ, Eyford BA, Varghese M, Arora H, Munro L, Warda T, Pfeifer CG, Sowa A, Dickstein DR, Rumbell T, Jefferies WA, Dickstein DL (2023) The intracellular domain of major histocompatibility class-I proteins is essential for maintaining excitatory spine density and synaptic ultrastructure in the brain. *Sci Rep* 13(1):6448. 10.1038/s41598-023-30054-8



23. Lazarczyk MJ, Kemmler JE, Eyford BA, Short JA, Varghese M, Sowa A, Dickstein DR, Yuk FJ, Puri R, Biron KE, Leist M, Jefferies WA, Dickstein DL (2016) Major Histocompatibility Complex class I proteins are critical for maintaining neuronal structural complexity in the aging brain. *Sci Rep* 6:26199. 10.1038/srep26199
24. Length RV (2022) emmeans: estimated marginal means, aka least squares means. R package version 1.7.0
25. Makale MT, McDonald CR, Hattangadi-Gluth JA, Kesari S (2017) Mechanisms of radiotherapy-associated cognitive disability in patients with brain tumours. *Nat reviews Neurol* 13(1):52–64. 10.1038/nrneurol.2016.185
26. Mizumatsu S, Monje M, Morhardt D, Rola R, Palmer T, Fike J (2003) Extreme sensitivity of adult neurogenesis to low doses of X-irradiation. *Cancer Res* 63(14):4021–4027
27. Montay-Gruel P, Acharya MM, Petersson K, Alikhani L, Yakkala C, Allen BD, Ollivier J, Petit B, Jorge PG, Syage AR, Nguyen TA, Baddour AAD, Lu C, Singh P, Moeckli R, Bochud F, Germond JF, Froidevaux P, Bailat C, Bourhis J, Vozenin MC, Limoli CL (2019) Long-term neurocognitive benefits of FLASH radiotherapy driven by reduced reactive oxygen species. *Proc Natl Acad Sci U S A* 116(22):10943–10951. 10.1073/pnas.1901777116
28. Montay-Gruel P, Petersson K, Jaccard M, Boivin G, Germond JF, Petit B, Doenlen R, Favaudon V, Bochud F, Bailat C, Bourhis J, Vozenin MC (2017) Irradiation in a flash: Unique sparing of memory in mice after whole brain irradiation with dose rates above 100Gy/s. *Radiother Oncol* 124(3):365–369. 10.1016/j.radonc.2017.05.003
29. Murcia-Belmonte V, Esteban PF, Martinez-Hernandez J, Gruart A, Lujan R, Delgado-Garcia JM, de Castro F (2016) Anosmin-1 over-expression regulates oligodendrocyte precursor cell proliferation, migration and myelin sheath thickness. *Brain Struct function* 221(3):1365–1385. 10.1007/s00429-014-0977-4
30. Parihar VK, Allen BD, Caressi C, Kwok S, Chu E, Tran KK, Chmielewski NN, Giedzinski E, Acharya MM, Britten RA, Baulch JE, Limoli CL (2016) Cosmic radiation exposure and persistent cognitive dysfunction. *Sci Rep* 6:34774. 10.1038/srep34774
31. Parihar VK, Limoli CL (2013) Cranial irradiation compromises neuronal architecture in the hippocampus. *Proc Natl Acad Sci U S A* 110(31):12822–12827. 10.1073/pnas.1307301110
32. Parihar VK, Pasha J, Tran KK, Craver BM, Acharya MM, Limoli CL (2015) Persistent changes in neuronal structure and synaptic plasticity caused by proton irradiation. *Brain Struct function* 220(2):1161–1171. 10.1007/s00429-014-0709-9
33. Price KA, Varghese M, Sowa A, Yuk F, Brautigam H, Ehrlich ME, Dickstein DL (2014) Altered synaptic structure in the hippocampus in a mouse model of Alzheimer's disease with soluble amyloid-beta oligomers and no plaque pathology. *Mol Neurodegener* 9:41. 10.1186/1750-1326-9-41
34. Seigers R, Fardell JE (2011) Neurobiological basis of chemotherapy-induced cognitive impairment: a review of rodent research. *Neurosci Biobehav Rev* 35(3):729–741 doi:S0149-7634(10)00146-6 [pii]. 10.1016/j.neubiorev.2010.09.006

35. Selkoe DJ (2002) Alzheimer's disease is a synaptic failure. *Science* 298(5594):789–791. 10.1126/science.1074069
36. Sholl DA (1953) Dendritic organization in the neurons of the visual and motor cortices of the cat. *J Anat* 87(4):387–406
37. Steele J, Brautigam H, Short J, Sowa A, Shi M, Yadav A, Weaver C, Westaway D, Fraser P, St. George-Hyslop P, Gandy S, Hof P, Diskstein D (2014) Early fear memory defects are associated with altered synaptic plasticity and molecular architecture in the TgCRND8 Alzheimer's mouse model. *J Comp Neurol* In
38. Tofilon PJ, Fike JR (2000) The radioresponse of the central nervous system: a dynamic process. *Radiat Res* 153(4):357–370
39. van Praag H, Schinder AF, Christie BR, Toni N, Palmer TD, Gage FH (2002) Functional neurogenesis in the adult hippocampus. *Nature* 415(6875):1030–1034
40. Vogel-Ciernia A, Matheos DP, Barrett RM, Kramar EA, Azzawi S, Chen Y, Magnan CN, Zeller M, Sylvain A, Haettig J, Jia Y, Tran A, Dang R, Post RJ, Chabrier M, Babayan AH, Wu JI, Crabtree GR, Baldi P, Baram TZ, Lynch G, Wood MA (2013) The neuron-specific chromatin regulatory subunit BAF53b is necessary for synaptic plasticity and memory. *Nat Neurosci* 16(5):552–561. 10.1038/nn.3359
41. Wefel JS, Schagen SB (2012) Chemotherapy-related cognitive dysfunction. *Curr Neurol Neurosci Rep* 12(3):267–275. 10.1007/s11910-012-0264-9

## Figures

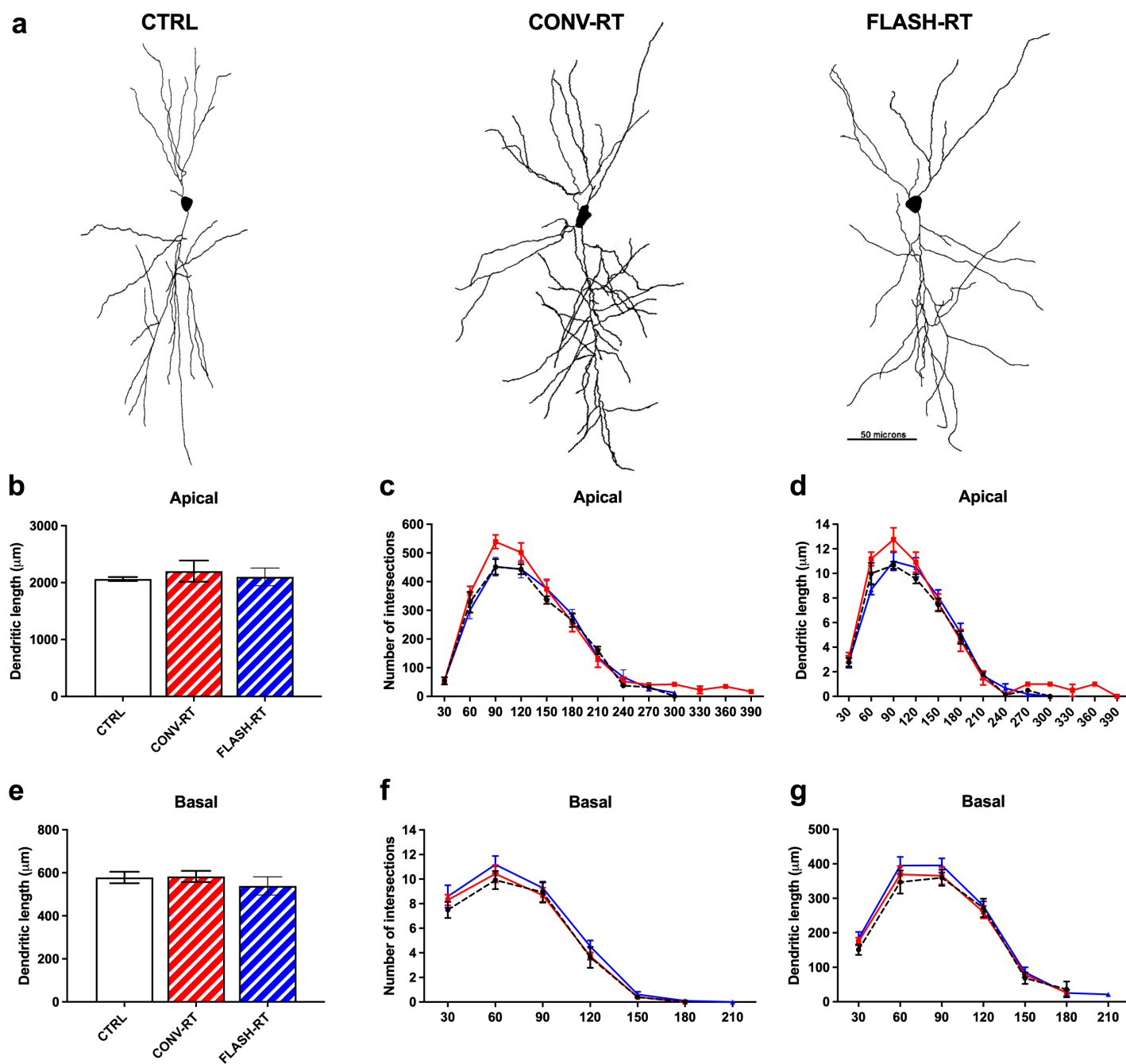


**Figure 1**

**10 Gy of irradiation did not affect neuronal complexity.** (a) Representative cell tracings from each treatment group. Scale bar 50  $\mu\text{m}$ . (b) Analysis of apical dendritic length. (c,d) Sholl analyses of apical dendrites. (e) Analysis of basal dendritic length. (f,g) Sholl analyses of basal dendrites. Data represent mean  $\pm$  SEM.

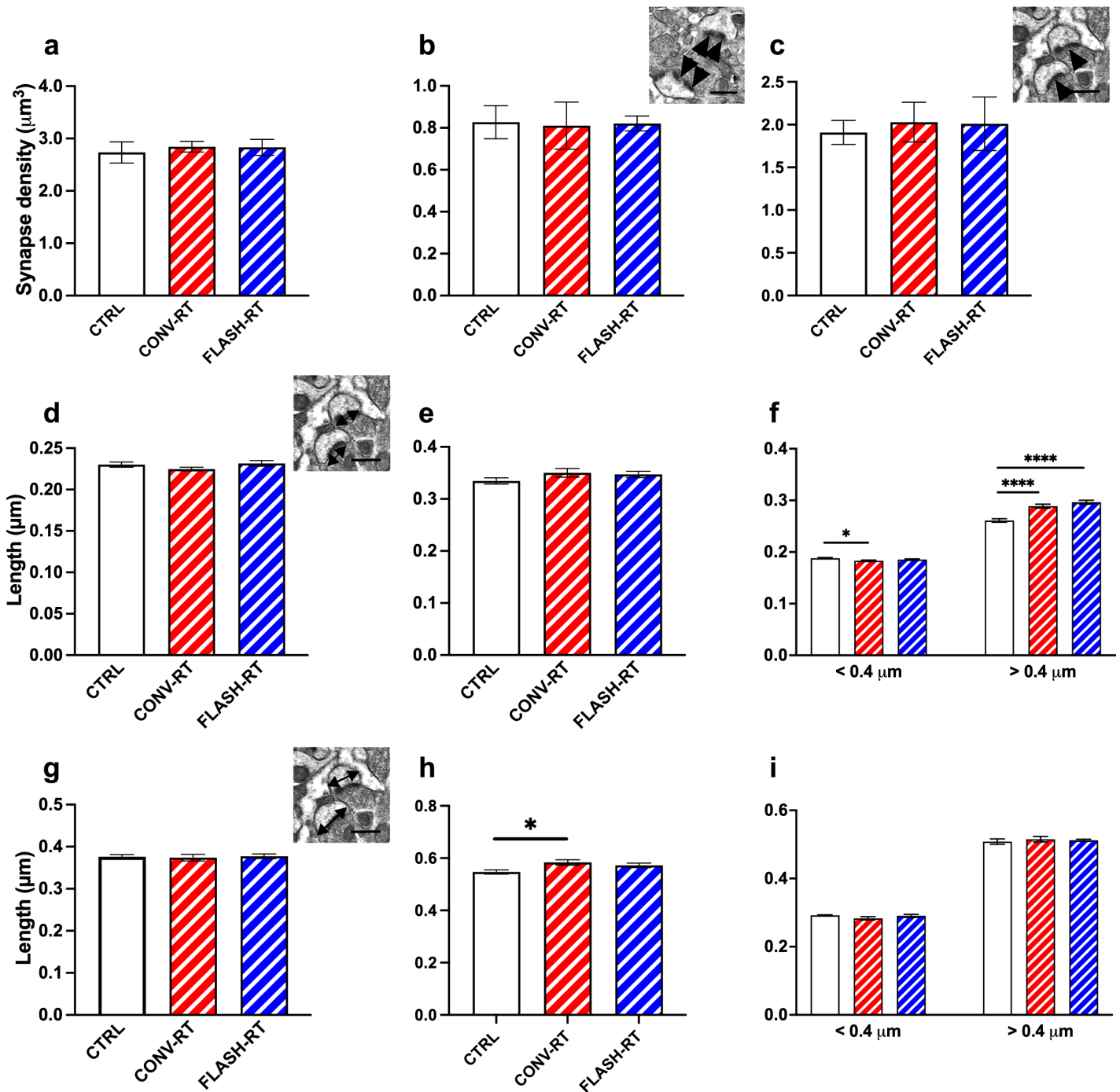


**Figure 2**

**Radiation treatment affect PSD size and synapse diameter in the CA1 region of the hippocampus.** There is no significant difference in **(a)** total synapse density, **(b)** perforated and **(c)** nonperforated synapse density. Inset images depict perforated synapses (arrowheads in **b**) and nonperforated synapses (arrowheads in **c**). Morphological analysis of synapses did not reveal significant differences in overall PSD length **(d)**, or PSD length in perforated synapses **(e)**, however, there were significant differences in smaller non-perforated synapses **(g)**. We did not observe any differences in spine head diameter in total synapses **(g)** however, when broken into perforated synapses **(h)** and non-perforated synapses **(i)** we found that perforated synapses in the CONV treated mice having larger head diameters than controls.

Inset images depict PSD length (arrows in **e**) and spine head diameter (arrows in **f**). Inset images depict PSD length in (**d**) and head diameter in (**g**). Data represents group mean  $\pm$  SEM. \* $p < 0.05$ , \*\*\*\* $p < 0.0001$ .

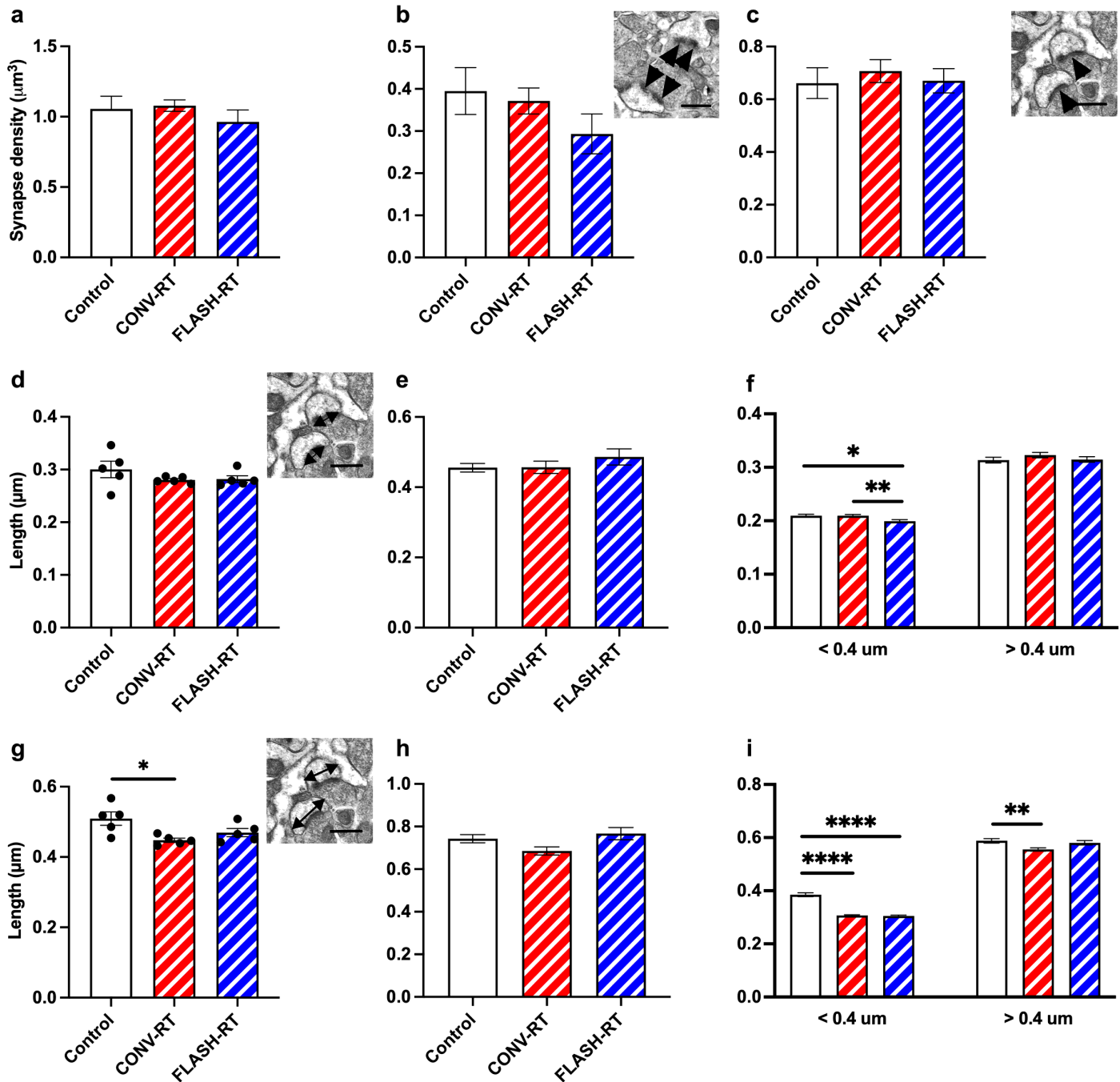


**Figure 3**

**Radiation treatment affects PSD size and synapse diameter in the mPFC.** There is no significant difference in (**a**) total synapse density, (**b**) perforated and (**c**) nonperforated synapse density. Inset images depict perforated synapses (arrowheads in **b**) and nonperforated synapses (arrowheads in **c**). Morphological analysis of synapses did not reveal significant differences in overall PSD length (**d**), or PSD length in perforated synapses (**e**), however, there was significant differences in smaller non-perforated synapses (**g**). We did see significant decrease in spine head diameter in total synapses (**g**)

however, when broken into perforated synapses (h) and non-perforated synapses (i) we only saw differences in non-perforated synapses with irradiated animals having smaller head diameters than sham controls. Inset images depict PSD length in (d) and head diameter in (g). Data represents group means  $\pm$ SEM.  $**p < 0.01$ ,  $****p < 0.0001$ .

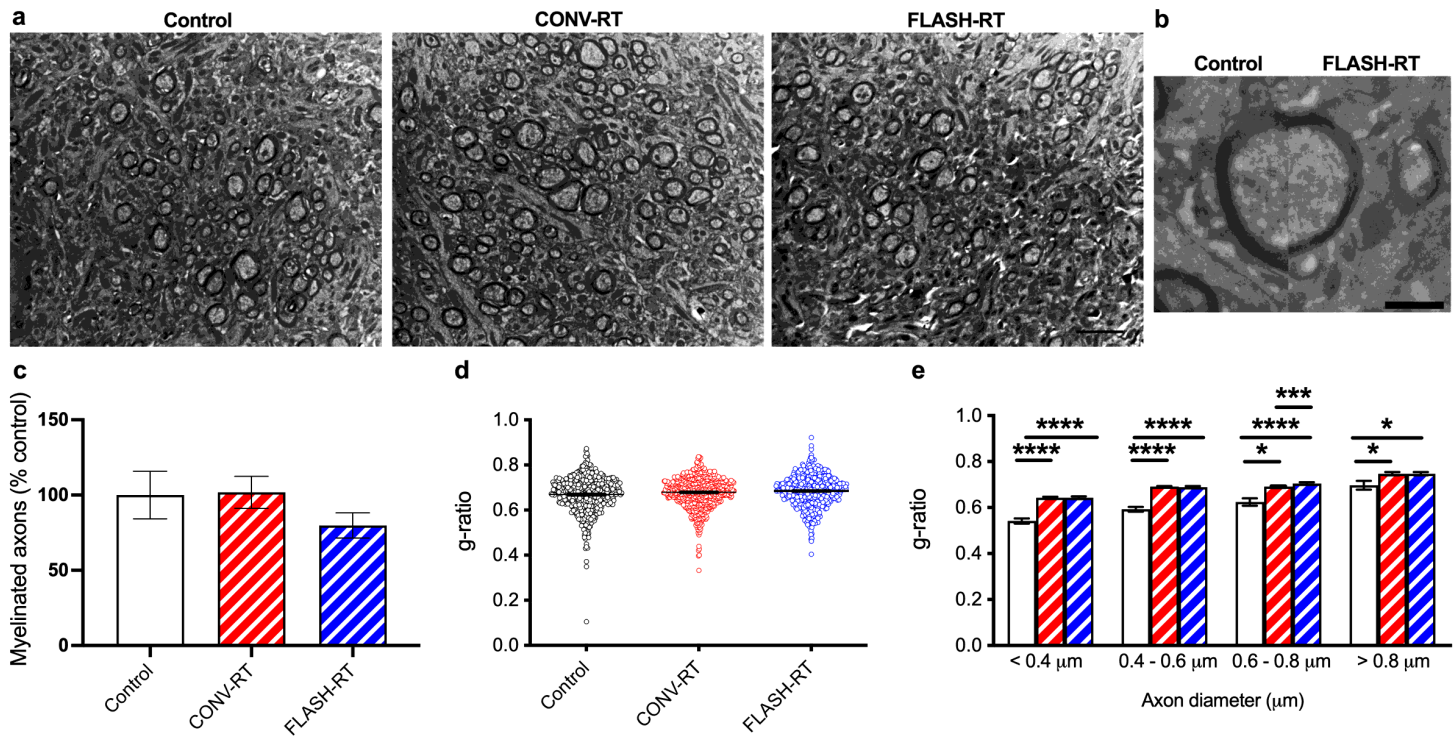


**Figure 4**

**Radiation treatment results in a decrease in axon myelin sheath thickness.** (a) Representative myelin images from all treatment groups. Scale bar = 500 nm. (b) Electron micrograph depicting a single axon of similar diameter in control mice (left) and FLASH mice (right). Scale bar 50 nm. (c) There was no significant difference in the percentage of myelinated axons between CONV, FLASH and control groups. Data represents group means  $\pm$  SEM. Overall g-ratios are larger in radiation treated mice compared to controls (d) and when binned according to axon diameter (e). Data represents individual measurements  $\pm$  SEM.  $*p < 0.05$ ,  $**p < 0.01$ ,  $***p < 0.001$ ,  $****p < 0.0001$ .



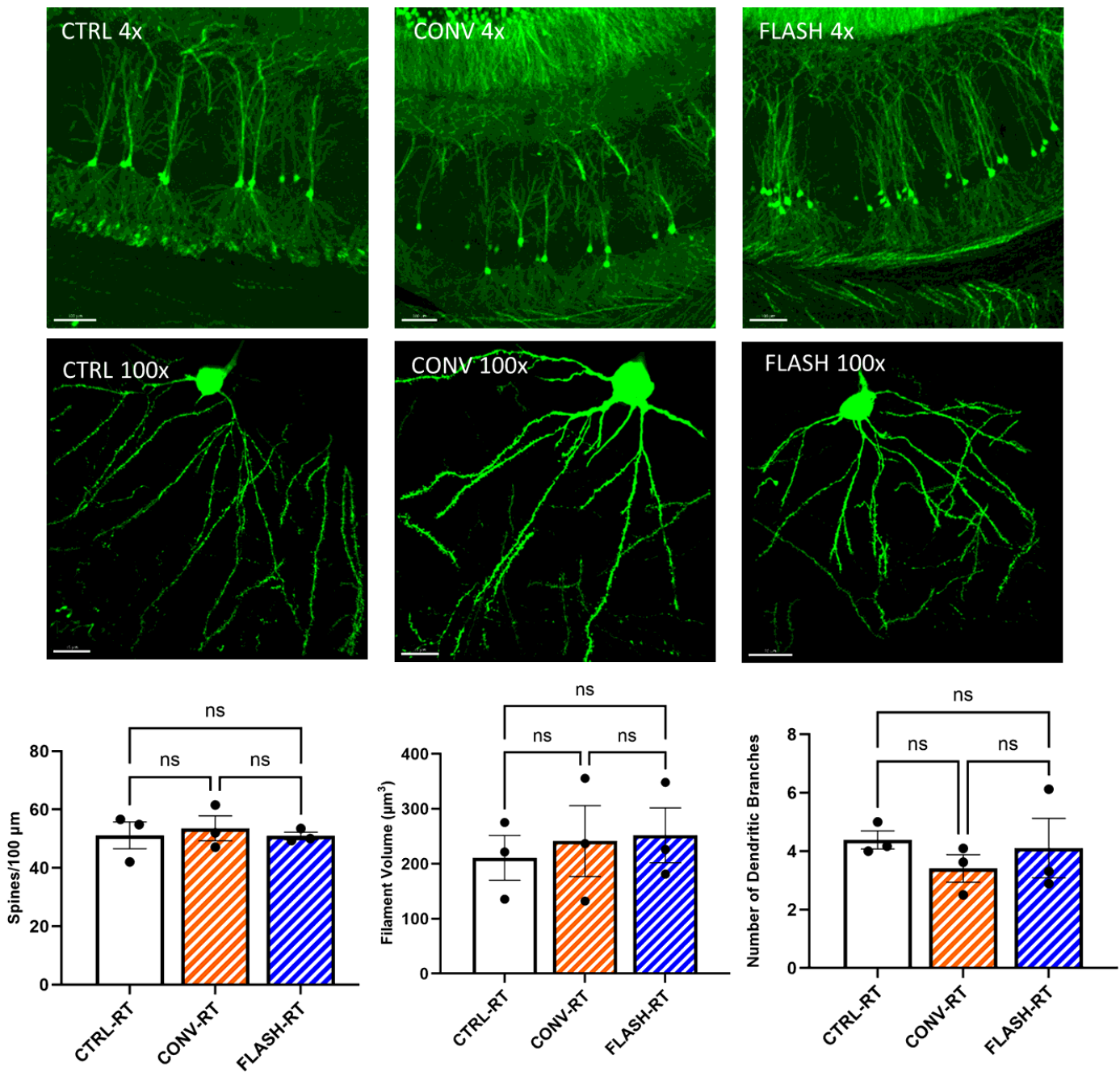


**Figure 5**

Cranial irradiation did not impact CA1 pyramidal neuron morphology and spine density in the Thy1-eGFP transgenic brains of mice exposed to either CONV or FLASH irradiation. (A-B) Representative full view z stacks of CA1 pyramidal neurons showing eGFP+-fluorescent apical dendrites emanating through the CA1 *stratum radiatum*. Scale bars 400  $\mu\text{m}$  and 15  $\mu\text{m}$ , respectively. (C) 3D algorithm-based filament and volumetric quantification of apical dendrite spine density, number of dendritic branches and filament volumes showed no significant differences between Control (CTRL), CONV and FLASH RT. Data represent mean  $\pm$  SEM (N=3 mice/group). One-way ANOVA.

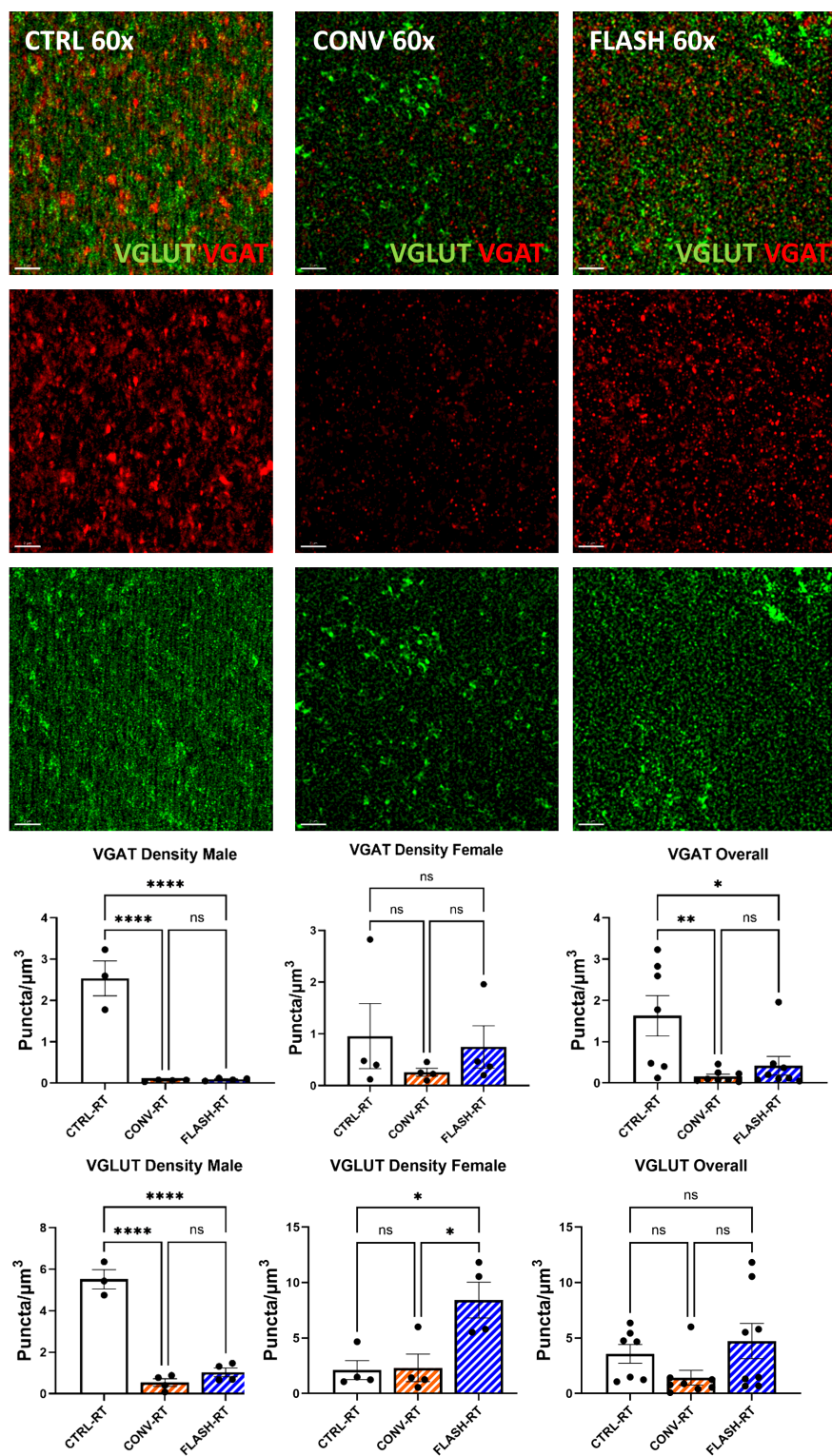


Figure 6

Super resolution microscopy analysis of excitatory and inhibitory synaptic vesicles (VGLUT, VGAT) post-CONV and FLASH dose-rate irradiations. (A) Representative full view z stacks of VGAT (Red) and VGLUT (Green) immunostaining within the CA1 *stratum radiatum* of Thy1-eGFP mice exposed to 0 Gy (CTRL), CONV and FLASH irradiation (Scale bar 2  $\mu\text{m}$ ). 3D algorithm-based volumetric quantification of VGAT<sup>+</sup> (B) and VGLUT<sup>+</sup> (C) immunoreactive puncta showed significant declines compared to the unirradiated



CTRL group ( $p < 0.0001$ ). Data represent mean  $\pm$  SEM (N=4 mice/group). One-way ANOVA followed by Bonferroni's multiple comparison. \* $p < 0.05$ , \*\* $p < 0.01$ , \*\*\*\* $p < 0.0001$ .